

Dielectrophoretically tunable optofluidic devices

This content has been downloaded from IOPscience. Please scroll down to see the full text.

2013 J. Phys. D: Appl. Phys. 46 483001

(<http://iopscience.iop.org/0022-3727/46/48/483001>)

View [the table of contents for this issue](#), or go to the [journal homepage](#) for more

Download details:

IP Address: 132.170.119.123

This content was downloaded on 12/11/2013 at 14:41

Please note that [terms and conditions apply](#).

TOPICAL REVIEW

Dielectrophoretically tunable optofluidic devices

Su Xu¹, Hongwen Ren² and Shin-Tson Wu¹¹ CREOL, The College of Optics and Photonics, University of Central Florida, Orlando, FL 32816, USA² Department of Polymer Nano-Science and Engineering, Chonbuk National University, Chonju, Chonbuk 561-756, Republic of South KoreaE-mail: swu@ucf.edu

Received 25 July 2013, in final form 18 September 2013

Published 7 November 2013

Online at stacks.iop.org/JPhysD/46/483001**Abstract**

Tunable optofluidic devices exhibit some unique characteristics that are not achievable in conventional solid-state photonic devices. They provide exciting opportunities for emerging applications in imaging, information processing, sensing, optical communication, lab-on-a-chip and biomedical engineering. A dielectrophoresis effect is an important physical mechanism to realize tunable optofluidic devices. Via balancing the voltage-induced dielectric force and interfacial tension, the liquid interface can be dynamically manipulated and the optical output reconfigured or adaptively tuned in real time. Dielectrophoretically tunable optofluidic devices offer several attractive features, such as rapid prototyping, miniaturization, easy integration and low power consumption. In this review paper, we first explain the underlying operation principles and then review some recent progress in this field, covering the topics of adaptive lens, beam steering, iris, grating, optical switch/attenuator and single pixel display. Finally, the future perspectives are discussed.

(Some figures may appear in colour only in the online journal)

1. Introduction

Conventional solid-state photonic devices have a remarkable optical performance and durability, but minimal adaptability. To achieve a high degree of adaptability, liquid is introduced as an optical interface. A new class of tunable optofluidic devices is thus emerging [1–4]. Extensive efforts have been devoted to this field since the mid-2000s and a large variety of tunable optofluidic devices brought into reality, for instance adaptive-focus lenses [5–26], beam steers [27, 28], gratings [29–31], irises [32–35], optical switches/attenuators [26, 36–41] and displays [41–47]. With a liquid-formed optical interface, such devices exhibit unique properties, which are not achievable in conventional solid-state photonic devices. Firstly, the optical interface (it can be a liquid–air or liquid–liquid interface) is intrinsically smooth because of the minimum interfacial energy, and thus mechanical polishing is not required. Secondly, the optical output can be reconfigured or adaptively tuned in real time through dynamically manipulating the

liquid interface. Thirdly, since the employed liquids are usually isotropic, these devices are polarization insensitive and broadband. Last but not least, if the device dimension is much smaller than the capillary length, the surface tension will dominate over the gravity, thus the devices will be vibration insensitive. Therefore, they provide exciting opportunities for emerging applications in imaging, information processing, sensing, optical communication, lab-on-a-chip and biomedical engineering. Various operation principles have been proposed to realize tunable optofluidic devices, e.g., fluidic pressure [14, 15, 32, 36], electrochemistry [16], thermal effect [11–13], environmentally adaptive hydrogel [9, 17, 18], electrowetting (EW) [19, 27, 34, 45–50] and dielectrophoresis (DEP) effect [20–26, 28–31, 35, 37–41, 43, 44].

The term *dielectrophoresis* was first introduced by Herbert Pohl in the early 1950s [51]. In his book, DEP is defined as the translational motion of neutral matter caused by polarization effects in a nonuniform electric field [51]. The force resulting from the polarization of the dielectric material is called Kelvin

polarization force or dielectric force. Unlike EW, DEP is a body-force phenomenon. For a bulky object, the dielectric force can be calculated by means of the polarization bulk force, in which the infinitesimal dipoles in an electric field experience a force that they pass on to the bulky object as a whole [52]. So far dielectric force has been implemented to manipulate biomolecules [53, 54], DNA [55], nanowires [56], nanotubes [57], microsized or nanosized dielectric droplets [58–60], lab-on-a-chip [61], micropumps [62, 63], micromotors [64], nanomechanical resonators [65], phase separation [66, 67], as well as to fabricate polymer microlens and gratings [31, 68, 69]. Recently, the realm has been extended to the manipulation of liquid–liquid interface, enabling a wide range of innovative tunable optofluidic devices, e.g., adaptive lenses [20–25], beam steers [28], irises [35], gratings [29–31], optical switches/attenuators [26, 37–41] and single pixel displays [41, 43, 44]. In comparison with the history of EW devices, DEP devices are still in their infancies. Several EW devices have been commercialized or close to commercial realizations. These two types of devices have some similarities. For instance, they usually employ two immiscible liquids in the cell, one liquid forms a droplet on the substrate and the other fills the surrounding area. They both use external voltage to tune the liquid–liquid interface: EW devices rely on the contact angle change between a conductive liquid and a solid surface; DEP devices rely on the net force exerted on polarizable dielectric liquids under a nonuniform electric field [70]. DEP tuning requires a higher actuation voltage, but consumes one order of magnitude less power [20]. Furthermore, electrolysis, Joule heating and microbubbles which always arise in EW devices [49] can be suppressed. Last but not least, EW devices often require expensive hermetic packaging (i.e. metal-glass packing) for long term operation due to the high saturated vapour pressure of the conductive liquid (e.g., salty water) [20], while DEP devices only need simple plastic packaging [71].

To optimize the performances of DEP devices from material aspects, there are some criteria to choose the liquids: they should be different in dielectric constants, immiscible with each other, non-toxic, stable and optically transparent for imaging applications. Other properties, such as refractive index and surface tension should also be taken into account for different applications. In addition to conventional isotropic liquids, liquid crystals (LCs) have also been adopted as the active media in optofluidic devices. LCs exhibit unique material properties ranging between those of conventional isotropic liquids and solid-state crystals. The most popular operating mechanism of LC devices is field-induced molecular reorientation, as reported by Schadt and Helfrich [72]. It enables today’s liquid crystal displays (LCDs), phase modulators, lenses, optical switches and other photonic LC devices. A relatively new mechanism which has recently attracted strong research attention is field-induced mechanical shape deformation of LC-droplets [39]. Via balancing the voltage-induced DEP forces and interfacial tensions, LC droplets expand or shrink upon voltage application. Based on this mechanism, novel electro-optical components beyond LCDs become feasible.

In this review, we will first explain the underlying operation principles to manipulate the shape of a dielectric

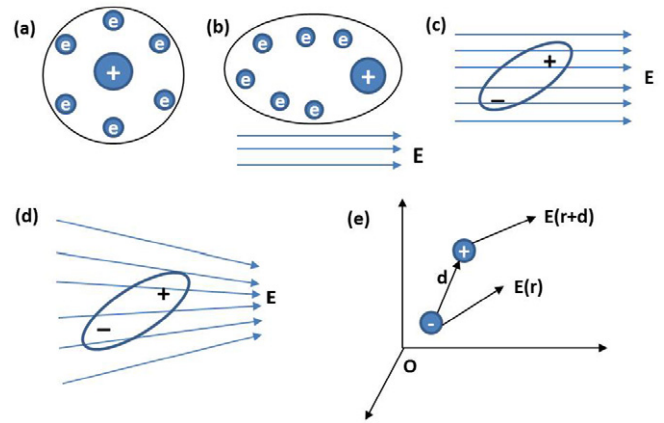


Figure 1. (a) Structure of a neutral particle or atom. (b) Electric field induced displacement of the charges. (c) A dielectric particle becomes polarized in a uniform electric field. (d) A dielectric particle in a nonuniform electric field. (e) Cartesian coordinate for deducing the electrostatic force.

liquid droplet. Then we will illustrate the recent progress on the development of dielectrophoretically tunable optofluidic (including both conventional isotropic liquids and LCs) devices by examples from recent literatures, covering topics of adaptive-focus lenses, beam steers, irises, gratings, optical switches/attenuators and single pixel displays. Future perspectives will also be discussed.

2. Basic principles

When a charged particle is placed in a homogeneous electric field, it experiences an electrostatic force as

$$\vec{f}_e = q \cdot \vec{E}, \quad (1)$$

where q is the net charge of the particle and \vec{E} is the electric field. However, if a charge-balanced particle is placed in such an electric field, the net electrostatic force is zero. A charge-balanced particle may be a dielectric particle or a neutral atom. In such a particle, a positively charged core is surrounded by a negatively charged electron cloud, as shown in figure 1(a). Its positive charge (+ Q) is equal to its negative charge ($-Q$). If the particle is subject to a homogeneous electric field, the nucleus is pushed in the direction of the electric field while the electrons are pushed in the opposite way (figure 1(b)). As a result, the charges undergo displacements and the particle becomes polarized. According to equation (1), the electrostatic force $+Q \cdot \vec{E}$ for the positive charge and $-Q \cdot \vec{E}$ for the positive charge are equal but in opposite direction, so the net force is zero. However, a dipole moment \vec{p} is induced. As figure 1(c) shows, in a simple case of two point charges, one with charge $+Q$ and the other with charge $-Q$, the induced electric dipole moment \vec{p} can be expressed as

$$\vec{p} = \lim_{Q \rightarrow \infty} \vec{d} \cdot Q, \quad (2)$$

where \vec{d} is the displacement vector pointing from the negative charge to positive charge, thus the electric dipole moment

vector \vec{p} points from the negative charge to the positive charge. Because of the induced dipole moment, this polar particle tends to rotate to line up its dipole moment parallel to the external electric field. A water molecule is a polar molecule. Even though the total charge on a water molecule is zero, the nature of chemical bonds is that the positive and negative charges do not completely overlap. Due to the separation of two positively charged hydrogen atoms and the negatively charged oxygen atom, water molecules possess a permanent dipole moment without the influence of external electric field. The dipole moments are permanent rather than induced. In addition to water molecules, some molecules such as chlorine, glycerol and ferroelectric LC molecules also have permanent dipole moments.

If the electric field is not *uniform*, the electric dipole of the particle experiences a net electric force because the positive charge $+Q$ is subject to an electric field that differs from the field acting on the negative charge $-Q$ (figure 1(d)). To deduce the electrostatic force acting on the particle, a Cartesian coordinate is established in figure 1(e). Positive charge $+Q$ and negative charge $-Q$ are separated by a distance \vec{d} , and the electric field at the $+Q$ and $-Q$ position is $\vec{E}(r+d)$ and $\vec{E}(r)$, respectively. The total force on the dipole is the sum of the forces on each individual charge, expressed as [73]

$$\begin{aligned} \vec{f}_e &= Q \cdot [\vec{E}(r+d) - \vec{E}(r)] = \vec{d} \cdot Q \cdot \frac{\vec{E}(r+d) - \vec{E}(r)}{\vec{d}} \\ &= \vec{p} \cdot \nabla \vec{E}, \end{aligned} \quad (3)$$

where \vec{p} is the dipole moment as defined in equation (2), $\nabla \vec{E}$ is the gradient of the electric field. From equation (3), it is obvious that in order to exert a net force on a dipole, the electric field has to be nonuniform. For a bulky object that cannot be simplified as an individual dipole, the polarization force acting on the object can be calculated by means of the polarization bulk force. From a microscopic view, the infinitesimal dipoles in an electric field experience a force that they pass on to the bulky object as a whole. Given the macroscopic polarization \vec{P} , the force density due to polarization is [74]

$$\vec{f}_{\text{KC}} = \vec{P} \cdot \nabla \vec{E}. \quad (4)$$

This is called Kelvin polarization force density or dielectric force density. Given the polarization of a linear dielectric material with a susceptibility χ_e ,

$$\vec{P} = \varepsilon_0 \chi_e \vec{E} = \varepsilon_0 (\varepsilon_r - 1) \vec{E} \quad (5)$$

the Kelvin polarization force density can be rewritten as

$$\vec{f}_d = \frac{1}{2} \varepsilon_0 (\varepsilon_r - 1) \nabla (\vec{E} \cdot \vec{E}). \quad (6)$$

If a dielectric object with a dielectric constant ε_d is surrounded by a dielectric medium with ε_m , equation (5) can be replaced by the excess polarization per unit volume

$$\vec{P} = \varepsilon_0 (\varepsilon_d - \varepsilon_m) \vec{E}. \quad (7)$$

Thus, the Kelvin polarization force density is

$$\vec{f}_{\text{KC}} = \frac{1}{2} \varepsilon_0 (\varepsilon_d - \varepsilon_m) \nabla (\vec{E} \cdot \vec{E}). \quad (8)$$

And the Kelvin polarization force or dielectric force exerted on a dielectric object with a volume V is expressed as [73, 74]

$$\vec{F}_{\text{KC}} = \int_V \frac{1}{2} \varepsilon_0 (\varepsilon_d - \varepsilon_m) \nabla (\vec{E} \cdot \vec{E}) dV. \quad (9)$$

From equation (9), the dielectric force is dependent on two terms: $\varepsilon_d - \varepsilon_m$ and the gradient of the electric field. If ε_d is equal to ε_m , then the dielectric force is zero. Also, the direction of the force is dependent on whether the object's dielectric constant is larger or smaller than that of the surrounding medium. Equation (9) explains the basic mechanism to manipulate the shape of a dielectric liquid droplet.

Compared with tunable optofluidic devices based on other techniques (e.g., fluidic pressure/electrochemistry/thermal effect/adaptive hydrogel/EW), those based on the DEP technique are becoming more and more attractive for practical applications in terms of (1) simple voltage driving, no complicated external control mechanisms (e.g., fluid circulation/mechanical movement/temperature) are required; (2) miniaturization and easy integration with existing electronic and microfluidic systems, thus functionally complex yet structurally simple systems (e.g., diagnostic or lab-on-chip applications) become feasible; (3) rapid prototyping and cost effectiveness; (4) low power consumption and (5) relatively low operating voltage and reasonably fast switching time.

In the following sections 3–8, we will illustrate the recent progress on the development of dielectrophoretically tunable optofluidic devices with examples, including adaptive-focus lenses, beam steers, irises, gratings, optical switches/attenuators and single pixel displays.

3. Adaptive-focus lenses

Conventional lenses are made of rigid glass or plastic, and thus they have a fixed optical power. To change the optical power, a zoom lens, which consists of at least two lenses with a tunable distance, is required. Such a stacking-lens system usually produces good image quality but is expensive, complex and delicate. The human eye is a natural type of adaptive liquid lens, in which the crystalline lens is constantly changing shape through ciliary muscles, allowing our eyes to clearly see objects at various distances. Adaptive liquid lenses mimic human eyes, by changing the surface shape through applying electric voltage [19–25], mechanical force [5–8], light [9, 10], and heat [11–13] to switch focus between distant and close-up objects in milliseconds. They are ‘smart’ and low-cost, yet high-quality alternatives to traditional rigid lenses. This topic has attracted significant research attention due to its tremendous potential in ophthalmology, machine vision, lighting, laser processing, optical communication and biomedical engineering.

An adaptive-focus liquid lens based on DEP effect usually employs two dielectric liquids with different dielectric constants: one liquid forms a lens droplet on the substrate and

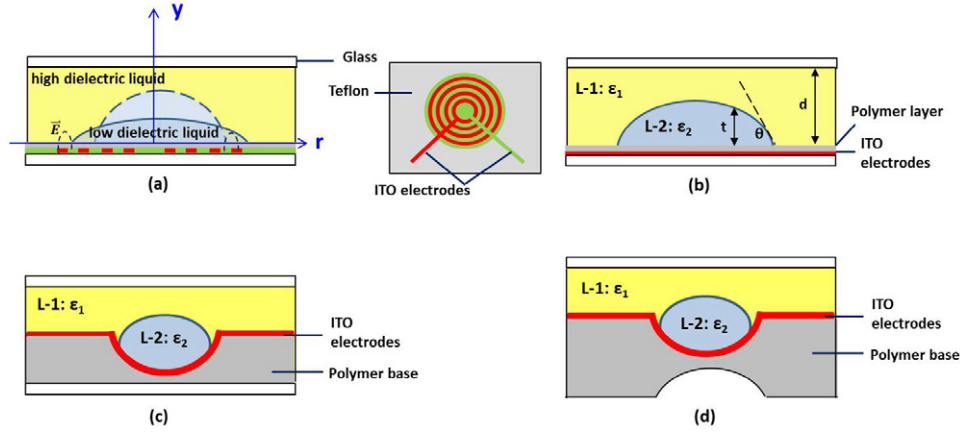


Figure 2. Side-view of (a) the dielectric liquid lens with concentric electrodes, (b) the dielectric liquid lens with planar ITO electrodes, (c) the dielectric liquid lens with a well-shaped electrode, and (d) the dielectric liquid lens with switchable positive and negative optical power.

another liquid fills the surroundings. Under an inhomogeneous electric field, the generated dielectric force deforms the liquid–liquid (or liquid–air) interface, which in turn changes the focal length. Upon removing the voltage, the droplet returns to the original shape because of the interfacial tension. Because of the interfacial tension, the shape of the liquid droplet is curved and its surface is very smooth. Like a deformed elastic membrane [75], if we consider the surface of the droplet as a very thin elastic membrane, then the shape of the droplet can be expressed as

$$y = \frac{1}{2} \left(\frac{P}{2S} \right) (a^2 - r^2) + \frac{1}{16} \left(\frac{P}{2S} \right)^3 (a^4 - r^4) + \dots \quad (10)$$

where y is the vertical axis and r is the horizontal axis passing through the droplet centre, as shown in figure 2(a). At $y = 0$, $r = a$ (a is the radius of droplet aperture). The droplet experiences a surface tension S and a pressure force P . When the droplet radius is small, we can neglect the higher order terms in equation (10) and only keep the first item, which implies that the droplet presents a parabolic shape. When the droplet is activated, the external voltage causes the pressure force P to increase, which in turn changes the droplet’s shape. However, the droplet still keeps a parabolic shape.

Cheng *et al* demonstrated the first DEP-driven LC droplet lens in 2006, in which LC was used as the high dielectric medium and the gradient electric field was introduced by concentric indium tin oxide (ITO) electrodes on the bottom substrate [20], as figure 2(a) shows. Teflon was coated on the electrodes to increase the contact angle of the LC droplet. Here the employed LC material needs to be in the isotropic phase, otherwise image blurring resulted from the LC birefringence will occur. Therefore, the operation temperature must be higher than the transition temperature between the nematic phase and the isotropic phase. To overcome such a problem, later an isotropic liquid droplet with a low dielectric constant and a sealing liquid with a high dielectric constant were adopted [21]. These two liquids possessed a wide temperature range of isotropic liquid phase over 150 °C. Moreover, they are density matched to minimize the gravitational effect and reduce the non-uniform deformation of the droplet profile. If a

density difference cannot be avoided, the lens shape should be maintained at a scale much smaller than the capillary length [76]. The focal length of a lens with 3 mm aperture can be tuned from 34 mm to 12 mm in the range 0–200 V_{rms} . Rise and fall times are 650 ms and 300 ms, respectively. Technically, the optical axis of the lens must remain intact at all operation modes, otherwise, the observed image will be distorted. Therefore, a coaxial design between the centre of the concentric electrodes and the optical axis of the liquid lens is critically important to maintain the optical functions. Cheng *et al* have proposed a planar liquid confinement structure along with concentric electrodes for the optical centring of dielectric liquid lenses at the rest state and actuated state [77]. During the actuation of an initially 7 mm diameter liquid lens, the tilt angle is measured to be 0.11° in maximum and below 0.03° during actuation. Yang *et al* investigated that a dielectric liquid droplet could achieve a fully developed contact angle change [78], which is distinct from the contact angle saturation behaviour of a conductive droplet actuated by EW.

To simplify the fabrication process, Ren *et al* demonstrated a lens using continuous flat electrodes in 2008 [22], as shown in figure 2(b). Under an applied voltage, the electric field exerted on the droplet can be expressed as

$$E_t = \frac{V/\varepsilon_2}{\frac{t}{\varepsilon_2} + \frac{d-t}{\varepsilon_1} + \frac{d_p}{\varepsilon_p}}, \quad (11)$$

where ε_1 , ε_2 and ε_p stand for the dielectric constant of liquid-1, liquid-2 and polymer layer, respectively; d is the cell gap, d_p is the thickness of polymer layer and t is the height of liquid-2 from the polymer layer to the curved surface of the droplet along the vertical direction (figure 2(b)). In equation (11) the influence of d_p/ε_p to E_t is negligible if the polymer layer is very thin ($d_p \rightarrow 0$). In this case, the electric field E_t near the droplet border can be expressed as

$$E_{t \rightarrow 0} = \frac{V\varepsilon_1}{d\varepsilon_2}. \quad (12)$$

If the apex distance of the droplet is approaching the cell gap ($t \rightarrow d$), then the electric field E_t at the apex position of the

droplet can be expressed as

$$E_{t \rightarrow d} = \frac{V}{d}. \quad (13)$$

If ϵ_1 is larger than ϵ_2 , the electric field at the border is ϵ_1/ϵ_2 times stronger than that at the apex position. Because the surface of the droplet changes continuously, the electric field has a gradient distribution. Therefore, the surface profile of the droplet can be reshaped by the generated dielectric force and the focal length can be tuned accordingly. In Ren's lens, liquid-1 and liquid-2 are Glycerol ($\epsilon_1 \sim 47, n_1 \sim 1.47, \rho_1 \sim 1.26 \text{ g cm}^{-3}$) and SantoLight™ Optical Fluids SL-5267 ($\epsilon_2 \sim 4.6, n_2 \sim 1.67, \rho_2 \sim 1.25 \text{ g cm}^{-3}$), respectively. The focal length of a lens with a $230 \mu\text{m}$ aperture diameter changes from $\sim 620 \mu\text{m}$ to $\sim 500 \mu\text{m}$ when the voltage increases to $90 V_{\text{rms}}$. The switching time (both contracting and relaxing) of the lens is $\sim 200 \text{ ms}$. In addition, a dielectric microlens array using a hole-patterned electrode has been demonstrated, but the droplets could drift in the lens cell, which degrades the lens's stability [23]. Such a problem also exists in dielectric lens with planar electrodes [21, 22]. Xu *et al* used a top planar electrode and a bottom well-shaped electrode to stabilize the position of the droplet, as well as lower the lens's operating voltage and broaden the lens's tuning range [24] (figure 2(c)). The curved polymer base was duplicated from a glass plano-convex microlens array. After coating a metal layer on the inner surface of the polymer base, it functions as a curved electrode. The focal length of a $700 \mu\text{m}$ aperture microlens can be tuned from $\sim 2.5 \text{ mm}$ to $\sim 1.39 \text{ mm}$ when the voltage increases from 0 to $88 V_{\text{rms}}$. Using different plano-convex microlens array stampers, microlens arrays with various apertures and filling factors can be easily fabricated. By patterning polymer micro-chambers on the planar electrode surface, a microlens array can be obtained as well [79]. The singlet microlens or microlens array has miscellaneous applications in lab-on-a-chip, imaging, beam diffuser, adaptive iris, light shutter and display.

The previously demonstrated dielectric lenses could only have pure positive or negative optical power [20–24]. A dielectric liquid microlens with switchable negative and positive optical power was illustrated in figure 2(d). The negative optical power induced by the bi-concave polymer base balances out the positive optical power of the liquid droplet to some extent, according to different operating voltage [25]. Hence, this lens can be continuously tuned among negative, zero and positive optical power states. The focal length of a $700 \mu\text{m}$ aperture microlens can be tuned from $\sim -7.56 \text{ mm}$ to infinity to $\sim 3.22 \text{ mm}$ when the voltage increases from 0 to $90 V_{\text{rms}}$. The response time is reasonably fast: $\sim 13 \text{ ms}$ in rising and $\sim 18 \text{ ms}$ in relaxing. The dimension of the bi-concave polymer base can be specially designed to get the desired lens's dynamic range. Such a liquid microlens will find potential applications in vision and imaging devices, especially in two dimensional (2D)-three dimensional (3D) displays [80].

The electro-optic characteristics study [81] and dynamic behaviour analysis [82] provide important insights into the effective actuation of the dielectric liquid lens. Researchers find that both amplitude and frequency of the voltage affect the

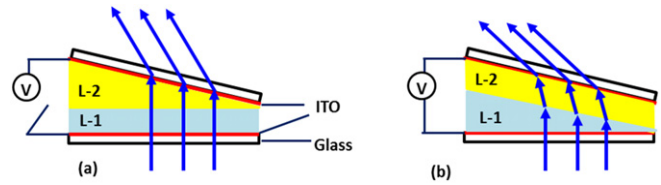


Figure 3. (a) Side-view of the device structure and (b) the beam steering by the tilted liquid–liquid interface.

droplet shape change. With the same amplitude of the applied voltage, a lower frequency can cause a larger shape change [81]. The viscosity and the droplet size are proportional to the response time. The applied ac frequency in the range 1–50 kHz is inversely proportional to the response time. The contact angles in equilibrium are found to be inversely proportional to the ac frequency and the droplet size but nearly invariant to the viscosity [82].

4. Beam steers

An inhomogeneous electric field can also be induced by two non-parallel substrates. A broadband and polarization-independent beam steering has been demonstrated by Lin *et al* in 2009 [28]. Both substrates are coated with continuous ITO electrodes. The top substrate is set slanted with an angle of 5° to the bottom substrate to generate a nonuniform electric field (figure 3(a)). Here L-1 is SL-5267 ($\epsilon_1 \sim 4.6, \gamma_1 \sim 50 \text{ mN m}^{-1}, \rho_1 \sim 1.25 \text{ g cm}^{-3}$) and L-2 is DI water ($\epsilon_2 \sim 80, n_2 \sim 1.33, \rho_2 \sim 1.0 \text{ g cm}^{-3}$). At $V = 0$, the liquid–liquid interface is horizontal and the beam propagates straightly. When the voltage is high enough, L-2 with a larger dielectric constant moves towards the region with a higher electric field intensity and squeezes L-1 to the right (figure 3(b)). As a result, the liquid–liquid interface becomes slanted and the beam is deflected. The maximum steering angle is $\sim 0.89^\circ$ at $V = 160 V_{\text{rms}}$. The rise time was 339 ms and the fall time 145 ms under $V = 110 V_{\text{rms}}$ (200 Hz square waves). The total transmittance of the lens system was $\sim 70\%$ at $\lambda = 633 \text{ nm}$. 2D beam steering can also be achieved by stacking two devices in orthogonal positions. The device has the potential for simple fabrication, broadband and 2D beam steering, polarization independence, simple control circuits, and cost effectiveness. Two technical challenges remain to be addressed: to keep a flat liquid–liquid interface at high operating voltages, and to reduce the operating voltage.

5. Gratings

Brown *et al* demonstrated an approach to produce static wrinkles at the surface of a thin oil film by dielectric force in 2009 [29]. Figure 4 illustrates the device structure. The glass substrate is successively coated with interdigitated striped electrodes and a thin dielectric layer (figure 4(a)). The electrode pitch p is $80 \mu\text{m}$. A small volume ($0.1 \mu\text{l}$) of 1-decanol ($\epsilon_{\text{oil}} = 8.1$) was dispensed onto the substrate and initially formed a spherical cap. When a voltage (20 kHz) was applied to the device, the oil experienced a dielectric force due

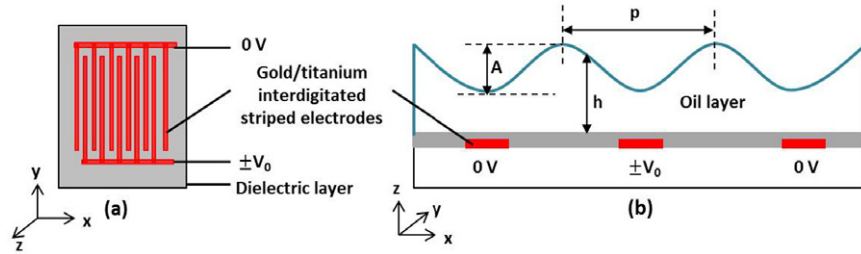


Figure 4. (a) The layout of the interdigitated electrodes and dielectric layer on the bottom substrate and (b) side view of the device structure.

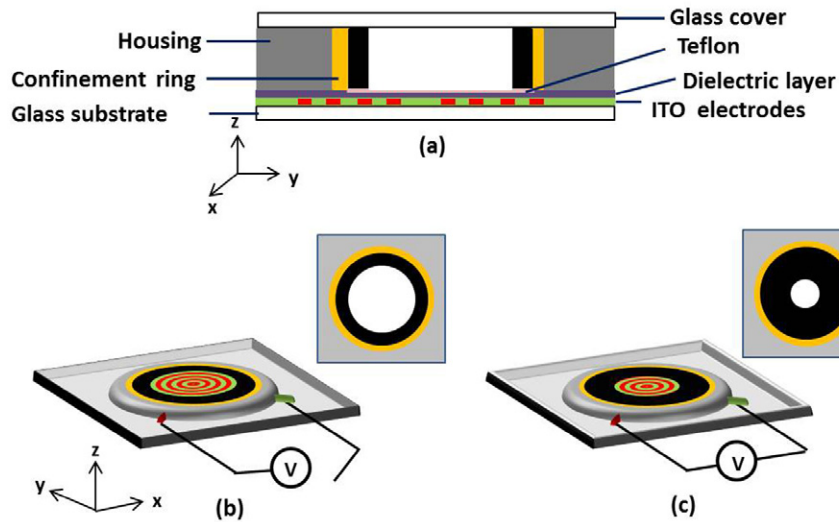


Figure 5. Structure of the dielectric liquid iris (a) side view, (b) top view at the rest state and (c) top view at the actuated state.

to the non-uniform electric fields generated by interdigitated striped electrodes. Because the dielectric constant of the oil is larger than that of the surrounding air, the dielectric force is along the direction of the increase in magnitude of the electric field. When the voltage exceeded $20 V_{\text{rms}}$, the oil was spread into a thin uniform film (thickness $h = 12 \mu\text{m}$) across the area with embedded electrodes by the dielectric force. Further increasing the voltage leads to a periodic undulation at the oil surface, and the period is equal to the electrode pitch. The peaks are located in the gaps between two adjacent electrodes where the highest electric field gradients occur (figure 4(b)). The peak-to-peak amplitude A increases with the voltage, it is $\sim 0.45 \mu\text{m}$ at $80 V_{\text{rms}}$ and $\sim 1.35 \mu\text{m}$ at $160 V_{\text{rms}}$. The period of the wrinkle can be adjusted using different electrode pitch.

Based on this operating mechanism, a switchable phase diffraction grating was demonstrated, in which the electrode pitch was $20 \mu\text{m}$ and the average film thickness $h = 3 \mu\text{m}$. As the voltage increased from 0 to $240 V_{\text{rms}}$, the orders were observed at angles of 0° (zero), 1.56° (+1) and 3.11° (+2), and the transition time between the zero and first order was below 40 ms. In addition to sinusoidal wrinkles with micrometre-scale pitches, more complex nonsinusoidal profiles with higher Fourier components were also generated using oil with a lower dielectric constant (hexadecane, $\epsilon_{\text{oil}} = 2.05$) and a longer electrode pitch ($p = 240 \mu\text{m}$). This work opens up the possibility of developing rapidly responsive voltage-programmable, polarization-insensitive transmission

and reflection diffraction devices and arbitrary surface profile optical devices.

6. Irises

A liquid iris diaphragm based on the DEP effect was demonstrated by Tsai *et al* in 2010 [35]. As figure 5(a) shows, it comprises four parts, including two immiscible liquids (transparent oil and an opaque ink), a substrate coated with concentric ITO electrodes, SU-8 dielectric layer and patterned Teflon layer, a glass cover, and polymethylmethacrylate (PMMA) housing with a hydrophilic confinement ring. The confinement ring and the concentric annular electrodes present a coaxial design; therefore, the centre axis of the iris can be always in a static position.

At the rest state, the surface area of the liquids interface is minimized due to the hydrophilic confinement ring and the hydrophobic Teflon film on the ITO electrode substrate (figure 5(b)). At an actuated state, the liquids experience an angularly symmetric electric fields induced by concentric annular electrodes, and the liquids interface suffers a dielectric force pointing to the centre, pulling the opaque ink inward (figure 5(c)). Such a state is stable when the dielectric force and the interfacial tensions reach a balance. Hence, the aperture size can be electrically tuned. It varies from 4 mm at the rest state to 1.5 mm at $160 V_{\text{rms}}$, and the corresponding aperture ratio is $\sim 62\%$. The transmittance was measured to exceed

85% without antireflection coatings over visible spectrum. The maximum electric power consumed is measured to be 5.7 mW. Compared with traditional mechanical irises, the dielectric liquid iris can continuously vary its aperture without any moving parts. It also overcomes the discrete variability of an electrophoresis-driven liquid iris [83], complicated external pumping system of a pressure-driven optofluidic iris [32] and high power consumption of EW type irises [33, 34, 84]. However, the operating voltage is quite high and the transmittance is relatively low (85%) compared with a mechanical iris with almost zero optical loss.

7. Optical switches

Optics communication networks require low loss, low cross talk, and highly reliable optical switches. Basically three types of optical switch have been proposed so far: mechanical, electro-optic and LC. The mechanical type, for example, uses tiny mirrors that reflect input signals and direct them to different ports. The operation of small-scale mechanical parts causes complications such as increased friction and long term wear. The electro-optical type has significantly large insertion losses and cross talk; LC-based type is polarization dependent. Optical switches using liquids as active medium have been extensively investigated, because liquids exhibit well defined and stable interfaces along with optical isotropy and high transmittance. Controlling the deformation or the movement of the liquids, the incoming light can be alternatively blocked or transmitted.

7.1. Optical switches based on reconfigurable liquid droplet

Wu's group has conducted series investigation and development of optical switches/attenuators based on DEP effect. Figure 6(a) shows the structure of an optical switch based on reconfigurable liquid droplet [38], which is similar to that of a dielectric lens (figure 2(b)). In a common dielectric liquid lens, the apex distance of the droplet is much smaller than the cell gap in order to prevent the dome of the droplet from touching the top substrate. If it touches the top substrate in a voltage-on state, the lens performance will be severely degraded and the droplet will no longer return to its original shape. When such a droplet is used for beam control, the controllability is rather limited and the required voltage is very high. To be distinct from a common dielectric liquid lens, here a small amount of liquid-1 (L-1, Glycerol, $\epsilon_1 \sim 47$, $\gamma_1 \sim 64 \text{ mN m}^{-1}$, $n_1 \sim 1.47$, $\rho_1 \sim 1.26 \text{ g cm}^{-3}$) with a fairly large surface tension forms a droplet on the bottom substrate; Liquid-2 (L-2, BK7 matching liquid, $\epsilon_2 \sim 5$, $\gamma_2 \sim 40 \text{ mN m}^{-1}$, $n_2 \sim 1.52$) with a relatively small surface tension fills the surrounding space. Continuous ITO electrodes are coated on the two substrates, on top of which is a thin dielectric layer ($\gamma_d \sim 40 \text{ mN m}^{-1}$). In the voltage-off state, the droplet is in a relaxing state. Its apex distance (t) is smaller than the cell gap (d). Since the refractive index of L-1 is smaller than that of L-2, a collimated incident beam will go divergent after passing the liquid droplet (figure 6(a)). As the voltage increases, the liquid droplet's dome is uplifted by the dielectric force and

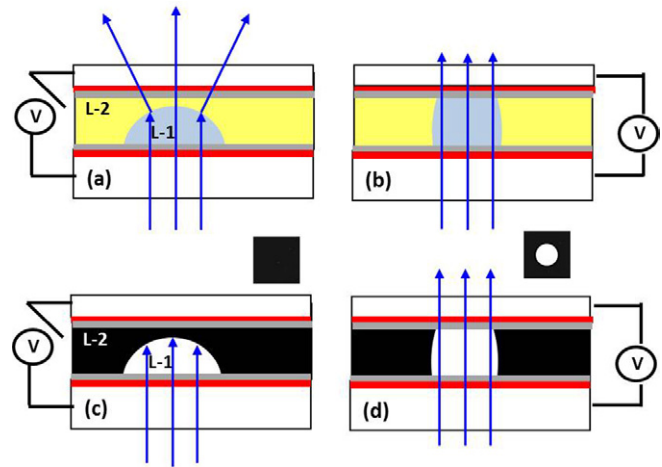


Figure 6. Operating mechanism of the optical switch based on a reconfigurable liquid droplet. Refractive type optical switch at (a) voltage-off state, (b) voltage-on state and absorption type optical switch at (c) voltage-off state and (d) voltage-on state.

touches the top substrate. The shape of the droplet is fixed under a given voltage and the beam can pass through the droplet without disturbance (figure 6(b)). Upon removing the voltage, the droplet will return to the original shape, because the surface tension of droplet L-1 is much larger than that of the top dielectric layer and L-2, the top dielectric layer is not strong enough to hold the droplet. Such an optical switch has a fairly low operating voltage. For a $150 \mu\text{m}$ aperture and $40 \mu\text{m}$ apex distance droplet, it touches the top substrate at $16 V_{\text{rms}}$ and the touching area reaches maximum at $35 V_{\text{rms}}$. The rise and decay times were measured to be $\sim 120 \text{ ms}$ and $\sim 180 \text{ ms}$, respectively, at $50 V_{\text{rms}}$.

If the transparent surrounding liquid is replaced by a black liquid (black dye doped LC mixture ZLI-2585, $\langle \epsilon \rangle \sim 7$, $\gamma \sim 20 \text{ mN m}^{-1}$), the incoming light will be blocked at the voltage-off state due to the absorption of black surrounding liquid (figure 6(c)) and transmitted at the voltage-on state (figure 6(d)) [37, 41]. For a large size beam control or optical switch, it is possible to fabricate a liquid droplet array using the cavity patterned method [79]. Different from a dielectric liquid lens [20–25], such an optical switch no longer depends on the refractive index difference, droplet profile and shape distortion. Therefore, its electro-optical performances, such as response time, can be easily improved by only considering a few criteria, e.g., viscosity and interfacial tensions.

7.2. Optical switches/attenuators based on voltage-stretchable LC droplet

In the optical switch shown in figure 6, the operating voltage increases with droplet size. It is a challenge to extremely expand the shape of a liquid droplet under a relatively low operating voltage using conventional approaches and materials [60, 85]. For most liquids with low surface tensions, their dielectric constants are usually very small ($\epsilon \sim 5$). While for the liquids with a large dielectric constant (such as water $\epsilon \sim 80$ and glycerol $\epsilon \sim 47$), their surface tensions are usually very high (over 60 mN m^{-1}) at room temperature. However,

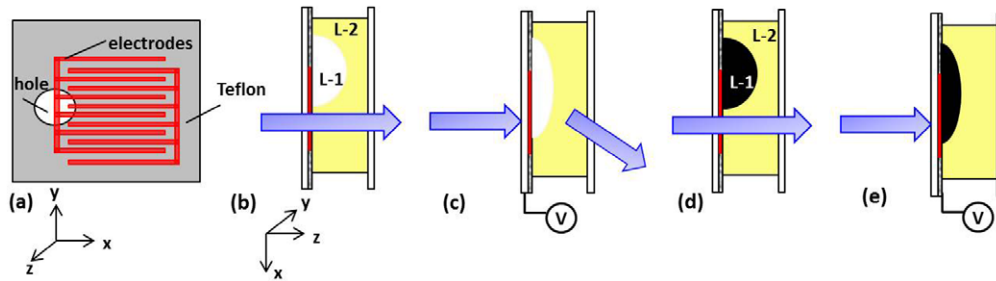


Figure 7. (a) The layout of the interdigitated ITO electrodes and Teflon layer on the bottom substrate. (The size of the hole and the width of electrode strips are not drawn by scale.), operating mechanism of the VOA based on voltage-stretchable LC droplet at (b) V-off state and (c) V-on state, and operating mechanism of the optical switch based on voltage-stretchable LC droplet at (d) V-off state and (e) V-on state.

some LC mixtures could have a large dielectric constant but a relatively small surface tension. Ren *et al* reported that employing interdigitated electrodes and an LC mixture with a large dielectric constant but small surface tension, the LC droplet can be extremely stretched along the electrodes at a relatively low voltage ($\sim 100 V_{\text{rms}}$) [39]. The droplet can also be stretched in both elongated and sidewise directions using a zigzag striped electrode. To further decrease the operating voltage, interdigitated ITO electrodes with a smaller electrode gap can be considered. Based on this finding, various optical switches/attenuators have been demonstrated.

Figures 7(a)–(c) show the structure of a variable optical attenuator (VOA) based on voltage-stretchable LC droplet. The LC droplet (L-1, Merck LC ZLI-4389, $\epsilon_{\parallel} = 56$, $\Delta\epsilon = 45.6$, $\gamma \sim 38 \text{ mN m}^{-1}$, $(n) \sim 1.58$, $\rho \sim 0.98 \text{ g m}^{-3}$) and the surrounding liquid (L-2, silicone oil, $\epsilon \sim 2.9$, $\gamma \sim 21 \text{ mN m}^{-1}$, $n \sim 1.4$, $\rho \sim 0.97 \text{ g cm}^{-3}$) are sandwiched between two glass substrates. The inner surface of the bottom substrate is coated with interdigitated ITO electrodes, on the top of which are a thin polyimide layer and a hole-patterned Teflon layer (figure 7(a)). These two layers not only provide a suitable contact angle for the droplet [86, 87] but also prevent the carrier injection into the cell. The hole partially contacts with the electrodes, pinning down the position of the droplet. At $V = 0$, the LC droplet shrinks with the smallest surface-to-volume ratio and the beam passes through the VOA without any deflection (figure 7(b)). When a voltage is applied to the bottom electrodes, a nonuniform lateral electric field is generated across the ITO stripes. As the voltage increases, the LC molecules at the droplet border near the bottom slab (within the penetration depth of the electric fields) are reoriented by the fringing field, leading to a much larger dielectric constant (close to $\epsilon_{\parallel} = 56$) than that of the silicone oil. Therefore, the LC near the bottom slab bears the strongest dielectric force. The force is pointed outwards, but only the horizontal component will deform the LC droplet. If the voltage is sufficiently high, the LC will be stretched outwards along the electrodes in order to reach a new balance between the interfacial tension and dielectric force. The stretched LC surface deflects the incident beam, leading to the attenuated transmission (figure 7(c)). Removing the voltage, the droplet will quickly return to its original state because of interfacial tension. The demonstrated VOA shows a broadband operation over the C-Band (1530–1560 nm), and $\sim 32 \text{ dB}$ dynamic range, $\sim 0.7 \text{ dB}$ insertion loss, $\sim 0.3 \text{ dB}$ polarization dependent loss

(PDL) and $\sim 20 \text{ ms}$ switching time at $\lambda = 1550 \text{ nm}$. The peak operating voltage is $\sim 40 V_{\text{rms}}$. Because the LC droplet is quite large (aperture $\sim 450 \mu\text{m}$, apex distance $\sim 200 \mu\text{m}$), thus even at $40 V_{\text{rms}}$ only a very thin LC layer (very close to the bottom substrate) is affected by the electric fields, while the bulk LC molecules are still randomly oriented. Therefore, this VOA keeps a small PDL at the effective working window.

An optical switch based on voltage-stretchable LC droplet was also demonstrated by doping black dyes into the LC droplet (L-1 in figure 7(d)) [39]. A collimated He–Ne laser beam is normally incident upon the ITO electrode area closely adjacent from the droplet (figure 7(d)). The beam goes through the cell with the highest transmittance at the voltage-off state. As the voltage increases, the beam is gradually blocked by the stretched LC droplet (figure 7(e)). For a cell with a 1.5 mm-aperture LC droplet, the highest intensity was measured to be ~ 0.72 and the lowest intensity in dark room was ~ 0.06 , leading to a contrast ratio of $\sim 120 : 1$ in transmissive mode. The expanding and relaxing time is, respectively, measured as $\sim 0.62 \text{ s}$ and $\sim 0.53 \text{ s}$ at a $50 V_{\text{rms}}$ (500 Hz) burst, and $\sim 0.17 \text{ s}$ and $\sim 0.83 \text{ s}$ at a $70 V_{\text{rms}}$ (500 Hz) burst. The expanding (relaxing) time is defined as the time needed from the contracted (stable stretched) shape to a stable stretched (contracted) shape. In such an optical switch, the operating voltage and response time depend on the travelling distance of the LC droplet. A longer travelling distance means a higher operating voltage and longer response time.

To solve these problems, an optical switch based on variable aperture was demonstrated [26]. The cross-sectional structure of the pixel is shown in figure 8(a). It consists of a bottom glass substrate, interdigitated ITO electrodes, a polymer hole, a ring-shaped liquid droplet and a top glass substrate. Both substrates are coated with Teflon. Figure 8(b) shows the top-view structure of the pixel, which is confined by a polymer hole (NOA65, $\gamma \sim 40 \text{ mN m}^{-1}$), and a liquid (black dye doped LC mixture ZLI-4389) forms a ring shape on the inside wall of the polymer hole due to the super hydrophobic Teflon layer coated on the top and bottom substrates. At $V = 0$, the pixel has the largest opening. When the voltage is high enough, instead of being stretched in one direction, the LC is stretched radially towards the centre of the pixel by the dielectric force, leading to a decrease in the aperture size (figures 8(c) and (d)). Upon removing the voltage, the stretched liquid returns to its initial state. The demonstrated optical switch has a pixel aperture of 0.23 mm, the thickness

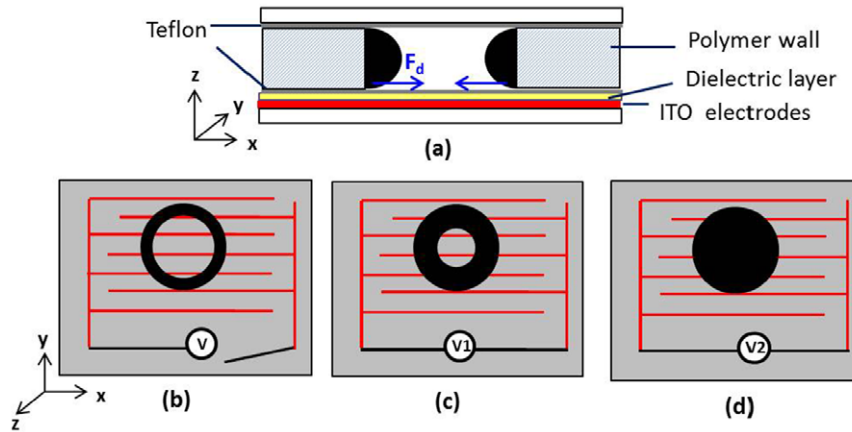


Figure 8. Structure and operating principle of optical switch based on variable aperture (a) side-view structure, (b) top view at $V = 0$, (c) at V_1 and (d) V_2 ($V_2 > V_1$).

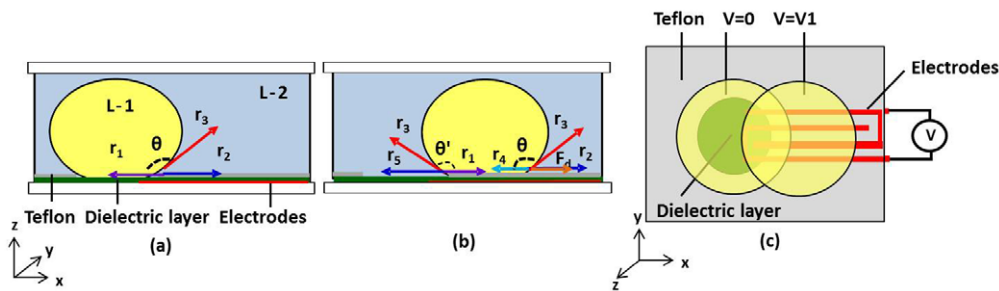


Figure 9. Device structure and operation mechanism. (a) The droplet pinned down on the hole surface at $V = 0$, (b) the droplet moved to the right side at $V = V_1$, and (c) the top view showing the position of the droplet at $V = 0$ and $V = V_1$. (The droplet size and electrode dimensions are not drawn by scale.)

of the polymer film is ~ 0.2 mm, and the filled LC occupies $\sim 20\%$ of its chamber space. The response time is ~ 10 ms at $80 V_{\text{rms}}$ and the aperture ratio is over 80%. It is found that when the pixel is totally covered by the LC, it has to wait for some time until the LC surface breaks up by itself. As a result, its response speed is slow. To ensure the stretched LC can return to its original state with fast response time, the stretched surface should not totally cover its aperture. For a large area optical switch or display, a two-dimensional pixel array can be simply fabricated.

7.3. Infrared optical switches based on position-shifting liquid droplet

With rapid development in optical communications, infrared (IR) light switch has become a key component for regulating the optical power in an optical system. Polymer dispersed liquid crystal (PDLC), which controls the incident light by scattering, has been proposed for IR light switch [88]. PDLC has some advantages, such as polarization independence, simple structure, and easy fabrication. However, due to the forward scattering, its optical attenuation is very sensitive to the distance between the device and the detector. Microfluidic devices have also been demonstrated to modulate IR light. Liquid flows into microchannels under a pressure and IR light is switched by manipulating the liquid's position [89, 90]. EW devices steer the IR light either by the total internal reflection

from a mercury slug [48] or by the deflection from a tunable liquid–liquid interface [91].

Ren *et al* demonstrated a simple IR light switch with a glycerol droplet actuated by a fringing field. In comparison with conventional liquids, glycerol has two unique merits: high absorption at $1.55 \mu\text{m}$ and large dielectric constant. The former enables the glycerol droplet to effectively evade or block the incident IR beam, while the latter helps to lower the operation voltage. Figure 9(a) shows the cross-sectional structure of the cell at $V = 0$. L-1 (Glycerol, $\epsilon_1 \sim 47$, $\gamma_1 \sim 64 \text{ mN m}^{-1}$, $\rho_1 \sim 1.26 \text{ g cm}^{-3}$) forms a droplet and L-2 (SL-5267, $\epsilon_2 \sim 4.6$, $\gamma_2 \sim 50 \text{ mN m}^{-1}$, $\rho_2 \sim 1.25 \text{ g cm}^{-3}$) fills the surrounding. At $\lambda = 1.55 \mu\text{m}$, L-1 is opaque while L-2 is transparent. To actuate the droplet, the inner surface of the bottom glass substrate is coated with interdigitated electrodes, followed by a thin dielectric layer and a thin Teflon layer sequentially. A hole, partially contacting with the edge of the striped electrodes, is patterned on the Teflon layer, pinning down the droplet position at the relaxed state. The electrode width and gap are $100 \mu\text{m}$ and $20 \mu\text{m}$, respectively, the cell gap is 5 mm. The diameter of the hole and the droplet aperture (the touching area on the bottom glass plate) is 3.5 mm and 4.5 mm, respectively. Due to the low surface tension of Teflon, the droplet exhibits a minimal surface-to-volume ratio on the Teflon surface.

When a voltage is applied, the droplet experiences a dielectric force and shifts rightwards to the region with high

electric field intensity (figure 9(b)). Once the droplet reaches a stable state, then along the ITO stripe direction, the system satisfies the following equation (14):

$$\gamma_1 + \gamma_2 + \cos \theta' \gamma_3 + F_d = \gamma_4 + \cos \theta \gamma_3 + \gamma_5 \quad (14)$$

where γ_1 , γ_2 , γ_3 , γ_4 and γ_5 denote the interfacial tension of L-1/dielectric layer, L-2/Teflon, and L-1/L-2, L-1/Teflon and L-2/dielectric layer, respectively; θ and θ' is the contact angle of L-1 on the Teflon surface and the dielectric layer, respectively; F_d is the horizontal component of dielectric force. From equation (14) as F_d increases, γ_4 and θ will change accordingly before the whole droplet totally shifts to the region with embedded electrodes. If the surface tension of the droplet is very large, the change of θ is rather limited. Instead, γ_4 will be the main varying factor because the droplet will go through a surface change from the dielectric layer surface to Teflon when it shifts rightwards. When the whole droplet is pulled to the region with embedded electrodes, it will stop shifting because the left side and right side of the droplet bears the same strength of the dielectric forces but in opposite directions (figure 9(c)). If the voltage is further increased, the droplet may be stretched along the striped electrodes in both directions, instead of only being shifted rightwards. Removing the voltage ($F_d = 0$), the droplet is pulled back to its original position by interfacial tensions. The alternation between the original state ($V = 0$) and the shifted state ($V = V_1$) can be used for light switch. For a 4.5 mm diameter droplet, the contrast ratio is over 95 : 1 in transmissive mode and response time is ~ 200 ms at 100 V_{rms} (1.5 kHz). The power consumption is less than ~ 1 mW. This IR switch can also work in reflective mode if the inner surface of the top glass substrate is coated with a reflector. This device concept can be extended to mid-wavelength IR [92] and long-wavelength IR [93] by choosing proper liquids in the desired spectral region.

8. Single pixel displays

LCDs have found widespread applications ranging from small panels (e.g. cell phones, portable video players and car navigations) to large-sized displays (e.g. computer monitors and TVs). The popularity arises from many of its advantages, including thin screen, lightweight, high definition, low driving voltages and low power consumption [94]. Generally speaking, an LCD panel consists of a two-dimensional array of pixels. Each pixel is driven independently by a thin film transistor (TFT). LCD is a non-emissive display so that it requires a backlight source. The LC cell is sandwiched between two crossed linear polarizers. Usually on the bottom substrate, a TFT array is formed to provide independent switch for each pixel. Transparent electrodes such as ITO are located at either TFT substrate or both substrates, depending on a specific LCD mode. With different voltages applied to ITO, the LC layer is switched and therefore different grey levels can be generated because of phase retardation. Colour filters are fabricated on the top substrate. By combining RGB colour filters with varied transmittance in each pixel, a full-colour display can be obtained [95]. Polarizers and colour filters

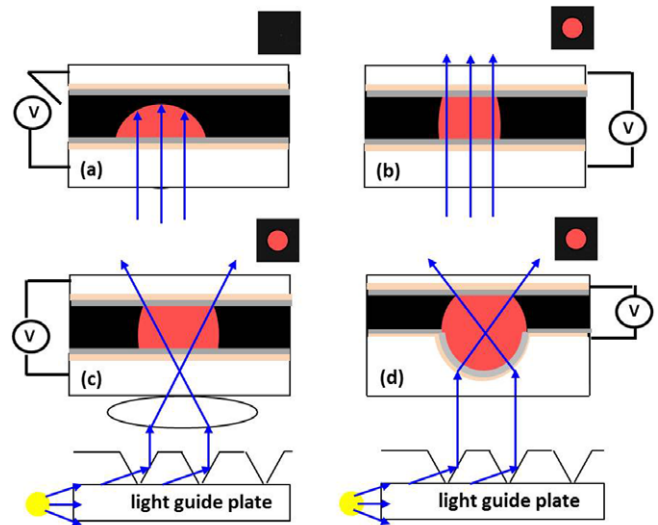


Figure 10. Side view structure of the pixel at (a) V-off state, (b) V-on state, (c) and (d) two approaches for obtaining a wide-view and high transmittance display through edge-lit backlight.

are the most critical components in today's LCDs, and they cannot be removed even though they are very expensive and cause poor optical efficiency. Many LC technologies, such as cholesteric LCs [96], dye-doped polymer-dispersed LCs [97] or dye-doped LC gels [98], and non-LC technologies, such as organic light-emitting diode (OLED) [99, 100], electrophoretic effect [101], EW [45, 46], electrofluidics [47], gyricon [102] and DEP [39, 41, 43, 44] have been proposed to achieve polarizer-free and colour filter-free displays.

8.1. Colour displays based on reconfigurable liquid droplet

This single pixel display has a same structure as that shown in figure 6(a). To make a red pixel, red dye-doped glycerol droplet and black dye-doped surrounding LC (ZLI-2585) are adopted (figure 10(a)). In the voltage-off state, the incident beam is absorbed by the black surrounding liquid, resulting in a dark state. As the voltage increases, the droplet dome is uplifted by the dielectric force and touches the top substrate. A dielectric effect-induced light channel is open and the incident beam is transmitted, thus a red pixel is observed. The liquid droplet returns to its initial state upon removing the voltage, and the pixel becomes dark again [26, 41, 43] (figure 10(b)). For the cell with a 130 μm aperture droplet and 100 μm gap, its contrast ratio is ~ 10 :1. At $V = 45 V_{\text{rms}}$ square-wave bursts, the rise time and decay time is measured as ~ 18 ms and ~ 32 ms, respectively.

In practical applications, a large-scale droplet array is required. These droplets should be separated by a patterned grid (such as black matrices) to avoid the crosstalk. A higher dye concentration and a larger distance between the droplet dome and the top surface would help us to improve the contrast ratio; however, the required voltage will be increased accordingly. A turning film and a microlens array are needed to redirect the backlight coming from the edge-lit system, widening the viewing angle and enhancing the light efficiency [103] (figure 10(c)). To further simplify the

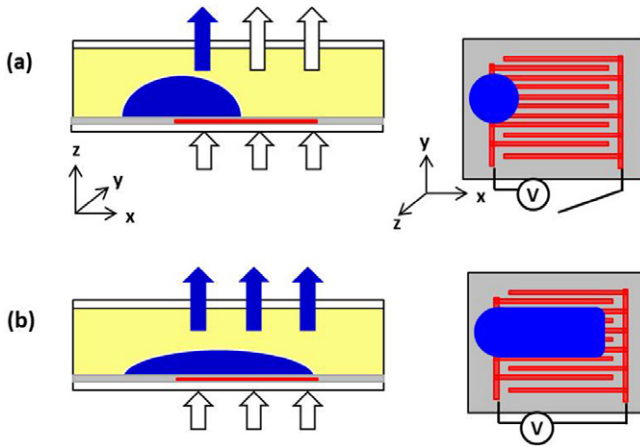


Figure 11. (a) Left: side view of the cell structure at V-off; right: top view of the cell structure at V-off, and (b) left: side view of the cell structure at V-on; right: top view of the cell structure at V-on.

system, a micro-lens embedded cell structure is introduced (figure 10(d)).

8.2. Colour displays based on voltage-stretchable liquid droplet

To resolve the problems of a single-pixel display based dielectric effect-induced light channel, a colour (black, red, blue) display based on voltage-stretchable LC droplet has been demonstrated [39, 44], as shown in figure 11. The device structure is very similar to that shown in figure 7. To achieve colour filter free, here the LC droplet (ZLI-4389) is doped with colour dyes and the surrounding silicone oil is clear. The droplet shrinks with the smallest surface-to-volume ratio at $V = 0$ (figure 11(a)). As the voltage increases, the droplet is stretched to spread like a film by the dielectric force, and the gray scale is achieved by stretching the droplet to a different extent (figure 11(b)). Upon removing the voltage, the droplet returns to its initial state. Such a device shows wide viewing angle, good contrast ratio and large aperture ratio, as well as easy integration with the edge-lit backlight. Both transmissive and reflective modes can be configured. For the pixel with an $800\ \mu\text{m}$ aperture droplet (doped with 1.2 wt% black dye) and $420\ \mu\text{m}$ gap, it has a $\sim 67\%$ aperture ratio and $\sim 83:1$ contrast ratio at $60\ V_{\text{rms}}$ (500 Hz). The expanding and recovering time are 260 ms and 500 ms, respectively, and the corresponding travel speeds are estimated to be $\sim 6.1\ \text{mm s}^{-1}$ and $\sim 3.2\ \text{mm s}^{-1}$, respectively. Such results are comparable to electrofluidic displays ($\sim 2.65\ \text{mm s}^{-1}$) [42]. For the pixel with a $500\ \mu\text{m}$ -aperture droplet (doped with 1.2 wt% red dye) and $400\ \mu\text{m}$ -gap, it has a $\sim 75\%$ aperture ratio at $50\ V_{\text{rms}}$ (500 Hz). The contrast ratio depends on the thickness of the area covered by LC and the dye concentration. A higher dye concentration will lead to a larger absorption even though the stretched LC layer is thin. The response time is governed by the liquid interfacial tension, flow viscosity, as well as travel distance. Surrounding liquid with low viscosity helps us to improve the travel speed.

Since a typical sub-pixel size of LCD is $\sim 240\ \mu\text{m} \times 80\ \mu\text{m}$, an $80\ \mu\text{m}$ aperture LC droplet would cover the whole

sub-pixel when it is stretched to $3\times$. Under the same travel speeds, the expanding and recovering time could be reduced to $\sim 26\ \text{ms}$ and $\sim 50\ \text{ms}$. To work in a reflective mode, a mirror was added as the reflector to the bottom substrate and the reflectance was measured to be $\sim 60\%$ (without AR coating).

9. Conclusions and outlook

This paper gives an overview of state of the art in dielectrophoretically tunable optofluidic devices. When a sessile droplet of a dielectric liquid is exposed to an inhomogeneous electric field, the surface of the droplet experiences a dielectric force, which reshapes the surface profile of the droplet until reaching a new equilibrium configuration. Two critical conditions are required to reshape the droplet: (1) a dielectric constant difference between the droplet and surrounding medium, and (2) an inhomogeneous electric field. Of particular interest we reported six types of photonic devices: lenses, beam steers, gratings, irises, optical switches and displays and explained their operating mechanisms. They are attractive for practical applications in terms of rapid prototyping, miniaturization, easy integration, low power consumption, polarization insensitivity, relatively low operating voltage as well as reasonably fast switching time. Such a combination of features in a single device is significantly comparable with existing technologies based on LCs, mechanics, electro-optics or acousto-optics.

To transfer the laboratory prototypes to commercial products, several technical challenges still need to be addressed. An important limitation is the choice of liquids.

When two dielectric liquids with different dielectric constants are chosen in the devices, other properties of the two liquids should be considered as well, such as refractive index, solubility, transmittance, density and surface tension. The highest refractive index of liquid is ~ 1.75 , which is much lower than that of solids. In addition, they have limited transparency in the IR range, especially in the $3\text{--}5\ \mu\text{m}$ and $8\text{--}12\ \mu\text{m}$, therefore, they are mostly used in the visible region. Since almost all physical properties of a liquid are temperature dependent, designing a liquid for a wide range of operating temperature is a big technical challenge. In comparison with EW devices, the operating voltage of DEP devices is relatively high at the right stage. A larger electric field gradient and a larger dielectric constant difference will help to further lower the operating voltage. Three types of electrodes have been reported in the literature to generate an inhomogeneous electric field. Planar electrodes and curved electrodes are more suitable to actuate micro-sized dielectric droplet, because a larger droplet needs a thicker cell gap to accommodate it, which means a higher operating voltage. Interdigitated-circular or -striped electrodes could generate an inhomogeneous fringing electric field. The significant advantage is that the driving voltage is independent of the cell gap. Innovative electrode designs to achieve low voltage driving are always desired.

In conclusion, by taking advantage of liquids' well-defined and stable interfaces along with optical isotropy and dielectric forces, a wide range of dielectrophoretically tunable optofluidic devices have been demonstrated. As the

advance of new dielectric liquid materials and novel electrode designs, their optical performances as well as the electro-optical properties are expected to be more competitive. In future, dielectrophoretically tunable optofluidic devices are foreseen to be low-cost yet high-quality alternatives to various conventional solid-state photonic devices, and play a key role in the optical systems for imaging, information processing, sensing, optical communication, lab-on-a-chip and biomedical engineering.

Acknowledgment

This work is partially supported by AFOSR under contract No FA95550-09-1-0170.

References

- [1] Psaltis D, Quake S R and Yang C 2006 Developing optofluidic technology through the fusion of microfluidics and optics *Nature* **442** 381–6
- [2] Monat C, Domachuk P and Eggleton B J 2007 Integrated optofluidics: a new river of light *Nature Photon.* **1** 106–14
- [3] Levy U and Shamai R 2008 Tunable optofluidic devices *Microfluid. Nanofluid.* **4** 97–105
- [4] Song W, Vasdekis A E and Psaltis D 2012 Elastomer based tunable optofluidic devices *Lab Chip* **12** 3590–7
- [5] Oku H and Ishikawa M 2009 High-speed liquid lens with 2 ms response and 80.3 nm root-mean-square wavefront error *Appl. Phys. Lett.* **94** 221108
- [6] Ren H, Fox D, Anderson P A, Wu B and Wu S-T 2006 Tunable-focus liquid lens controlled using a servo motor *Opt. Express* **14** 8031–6
- [7] Liu C-S and Lin P D 2009 Miniaturized auto-focusing VCM actuator with zero holding current *Opt. Express* **17** 9754–63
- [8] Son H-M, Kim M Y and Lee Y-J 2009 Tunable-focus liquid lens system controlled by antagonistic winding-type SMA actuator *Opt. Express* **17** 14339–50
- [9] Zeng X and Jiang H 2008 Tunable liquid microlens actuated by infrared light-responsive hydrogel *Appl. Phys. Lett.* **93** 151101
- [10] Xu S, Ren H, Lin Y-J, Moharam M G J, Wu S-T and Tabiryani N 2009 Adaptive liquid lens actuated by photo-polymer *Opt. Express* **17** 17590–5
- [11] Miccio L, Finizio A, Grilli S, Vespini V, Paturzo M, De Nicola S and Ferraro P 2009 Tunable liquid microlens arrays in electrode-less configuration and their accurate characterization by interference microscopy *Opt. Express* **17** 2487–99
- [12] Grilli S, Miccio L, Vespini V, Finizio A, De Nicola S and Ferraro P 2008 Liquid micro-lens array activated by selective electrowetting on lithium niobate substrates *Opt. Express* **16** 8084–93
- [13] Zhang W, Aljaseem K, Zappe H and Seifert A 2011 Completely integrated, thermo-pneumatically tunable microlens *Opt. Express* **19** 2347–62
- [14] Sugiura N and Morita S 1993 Variable-focus liquid-filled optical lens *Appl. Opt.* **32** 4181–6
- [15] Jeong K-H, Liu G, Chronis N and Lee L 2004 Tunable microdoublet lens array *Opt. Express* **12** 2494–500
- [16] Lopez C A, Lee C-C and Hirska A H 2005 Electrochemically activated adaptive liquid lens *Appl. Phys. Lett.* **87** 134102
- [17] Dong L, Agarwal A K, Beebe D J and Jiang H 2006 Adaptive liquid microlenses activated by stimuli-responsive hydrogels *Nature* **442** 551–4
- [18] Zhu D, Li C, Zeng X and Jiang H 2010 Tunable-focus microlens arrays on curved surfaces *Appl. Phys. Lett.* **96** 081111
- [19] Berge B and Peseux J 2000 Variable focal lens controlled by an external voltage: An application of electrowetting *Eur. Phys. J. E* **3** 159–63
- [20] Cheng C-C, Chang C A and Yeh J A 2006 Variable focus dielectric liquid droplet lens *Opt. Express* **14** 4101–6
- [21] Cheng C-C and Yeh J A 2007 Dielectrically actuated liquid lens *Opt. Express* **15** 7140–5
- [22] Ren H, Xianyu H, Xu S and Wu S-T 2008 Adaptive dielectric liquid lens *Opt. Express* **16** 14954–60
- [23] Ren H and Wu S-T 2008 Tunable-focus liquid microlens array using dielectrophoretic effect *Opt. Express* **16** 2646–52
- [24] Xu S, Lin Y-J and Wu S-T 2009 Dielectric liquid microlens with well-shaped electrode *Opt. Express* **17** 10499–505
- [25] Xu S, Ren H, Liu Y and Wu S-T 2011 Dielectric liquid microlens with switchable negative and positive optical power *J. Microelectromech. Syst.* **20** 297–301
- [26] Ren H, Xu S and Wu S-T 2012 Optical switch based on variable aperture *Opt. Lett.* **37** 1421–3
- [27] Smith N R, Abeysinghe D C, Haus J W and Heikenfeld J 2006 Agile wide-angle beam steering with electrowetting micropisms *Opt. Express* **14** 6557–63
- [28] Lin Y-J, Chen K-M and Wu S-T 2009 Broadband and polarization-independent beam steering using dielectrophoresis-tilted prism *Opt. Express* **17** 8651–6
- [29] Brown C V, Wells G G, Newton M I and McHale G 2009 Voltage-programmable liquid optical interface *Nature Photon.* **3** 403–5
- [30] Brown C V, Al-Shabib W, Wells G G, McHale G and Newton M I 2010 Amplitude scaling of a static wrinkle at an oil-air interface created by dielectrophoresis forces *Appl. Phys. Lett.* **97** 242904
- [31] Wells G G, Sampara N, Kriezis E E, Fyson J and Brown C V 2011 Diffraction grating with suppressed zero order fabricated using dielectric forces *Opt. Lett.* **36** 4404–6
- [32] Yu H, Zhou G, Siong C F and Lee F 2008 Optofluidic variable aperture *Opt. Lett.* **33** 548–50
- [33] Müller P, Feuerstein R and Zappe H 2012 Integrated Optofluidic Iris *J. Microelectromech. Syst.* **21** 1156–64
- [34] Murade C U, Oh J M, van den Ende D and Mugele F 2011 Electrowetting driven optical switch and tunable aperture *Opt. Express* **19** 15525–31
- [35] Tsai C G and Yeh J A 2010 Circular dielectric liquid iris *Opt. Lett.* **35** 2484–6
- [36] Yu H, Zhou G, Siong C F and Lee F 2008 A variable optical attenuator based on optofluidic technology *J. Micromech. Microeng.* **18** 115016
- [37] Ren H and Wu S-T 2010 Optical switch using a deformable liquid droplet *Opt. Lett.* **35** 3826–8
- [38] Ren H, Xu S and Wu S-T 2010 Deformable liquid droplets for optical beam control *Opt. Express* **18** 11904–10
- [39] Ren H, Xu S and Wu S-T 2011 Voltage-expandable liquid crystal surface *Lab Chip* **11** 3426–30
- [40] Xu S, Ren H, Sun J and Wu S-T 2012 Polarization independent VOA based on dielectrically stretched liquid crystal droplet *Opt. Express* **20** 17059–64
- [41] Ren H, Xu S, Ren D and Wu S-T 2011 Novel optical switch with a reconfigurable dielectric liquid droplet *Opt. Express* **19** 1985–90
- [42] Yang S, Zhou K, Kreit E and Heikenfeld J 2010 High reflectivity electrofluidic pixels with zero-power grayscale operation *Appl. Phys. Lett.* **97** 143501
- [43] Xu S, Ren H, Liu Y and Wu S-T 2011 71.2: Color displays using reconfigurable liquid droplets *SID Symp. Digest of Technical Papers (Los Angeles, CA)* vol 42, pp 1046–8

- [44] Xu S, Ren H, Liu Y and Wu S-T 2012 Color displays based on voltage-stretchable liquid crystal Droplet *J. Disp. Technol.* **8** 336–40
- [45] Hayes R A and Feenstra B J 2003 Video-speed electronic paper based on electrowetting *Nature* **425** 383–5
- [46] Blankenbach K, Schmoll A, Bitman A, Bartels F, Jerosch D 2008 Novel highly reflective and bistable electrowetting displays *J. Soc. Inf. Disp.* **16** 237–44
- [47] Heikenfeld J, Zhou K, Kreit E, Raj B, Yang S, Sun B, Milarcik A, Clapp L and Schwartz R 2009 Electrofluidic displays using Young–Laplace transposition of brilliant pigment dispersions *Nature Photon.* **3** 292–6
- [48] Jackel J L, Hackwood S and Beni G 1982 Electrowetting optical switch *Appl. Phys. Lett.* **40** 4–5
- [49] Vallet M, Berge B and Vovelle L 1996 Electrowetting of water and aqueous solutions on poly(ethylene terephthalate) insulating films *Polymer* **37** 2465–70
- [50] Frieder M and Jean-Christophe B 2005 Electrowetting: from basics to applications *J. Phys.: Condens. Matter* **17** R705–74
- [51] Pohl H A 1978 *Dielectrophoresis* (Cambridge: Cambridge University Press)
- [52] Schmid S, Hierold C and Boisen A 2010 Modeling the Kelvin polarization force actuation of micro- and nanomechanical systems *J. Appl. Phys.* **107** 054510
- [53] Weber A P, Seipenbusch M and Kasper G 2003 Size effects in the catalytic activity of unsupported metallic nanoparticles *J. Nanopart. Res.* **5** 293–8
- [54] Agastin S, King M R and Jones T B 2009 Rapid enrichment of biomolecules using simultaneous liquid and particulate dielectrophoresis *Lab Chip* **9** 2319–25
- [55] Regtmeier J, Duong T T, Eichhorn R, Anselmetti D and Ros A 2007 Dielectrophoretic manipulation of DNA: separation and polarizability *Anal. Chem.* **79** 3925–32
- [56] Smith P A, Nordquist C D, Jackson T N, Mayer T S, Martin B R, Mbindyo J and Mallouk T E 2000 Electric-field assisted assembly and alignment of metallic nanowires *Appl. Phys. Lett.* **77** 1399–401
- [57] Fung C K M, Wong V T S, Chan R H M and Li W J 2004 Dielectrophoretic batch fabrication of bundled carbon nanotube thermal sensors *IEEE Trans. Nanotechnol.* **3** 395–403
- [58] Jones T B, Gunji M, Washizu M and Feldman M J 2001 Dielectrophoretic liquid actuation and nanodroplet formation *J. Appl. Phys.* **89** 1441–8
- [59] Ahn K, Kerbage C, Hunt T P, Westervelt R M, Link D R and Weitz D A 2006 Dielectrophoretic manipulation of drops for high-speed microfluidic sorting devices *Appl. Phys. Lett.* **88** 024104
- [60] McHale G, Brown C V, Newton M I, Wells G G and Sampara N 2011 Dielectrowetting driven spreading of droplets *Phys. Rev. Lett.* **107** 186101
- [61] Zeng J and Kormsmeier T 2004 Principles of droplet electrohydrodynamics for lab-on-a-chip *Lab Chip* **4** 265–277
- [62] Laser D J and Santiago J G 2004 A review of micropumps *J. Micromech. Microeng.* **14** R35–64
- [63] Ren H, Xu S and Wu S-T 2013 Liquid crystal pump *Lab Chip* **13** 100–5
- [64] Hagedorn R, Fuhr G, Müller T, Schnelle T, Schnakenberg U and Wagner B 1994 Design of asynchronous dielectric micromotors *J. Electrostat.* **33** 159–85
- [65] Unterreithmeier Q P, Weig E M and Kotthaus J P 2009 Universal transduction scheme for nanomechanical systems based on dielectric forces *Nature* **458** 1001–4
- [66] Kim Y, Francl J, Taheri B and West J L 1998 A method for the formation of polymer walls in liquid crystal/polymer mixtures *Appl. Phys. Lett.* **72** 2253–5
- [67] Ren H, Wu S-T and Lin Y-H 2008 In situ observation of fringing-field-induced phase separation in a liquid-crystal–monomer mixture *Phys. Rev. Lett.* **100** 117801
- [68] Hung K-Y, Fan C-C, Tseng F-G and Chen Y-K 2010 Design and fabrication of a copolymer aspheric bi-convex lens utilizing thermal energy and electrostatic force in a dynamic fluidic *Opt. Express* **18** 6014–23
- [69] Hung K-Y, Chang L-W, Tseng F-G, Chiou J-C and Chiu Y 2010 Optimum electrostatic force control for fabricating a hybrid UV-curable aspheric lens *J. Micromech. Microeng.* **20** 075001
- [70] Jones T B 2002 On the relationship of dielectrophoresis and electrowetting *Langmuir* **18** 4437–43
- [71] Yang C-C, Tsai C G and Yeh J A 2010 Miniaturization of dielectric liquid microlens in package *Biomicrofluidics* **4** 043006
- [72] Schadt M and Helfrich W 1971 Voltage-dependent optical activity of a twisted nematic liquid crystal *Appl. Phys. Lett.* **18** 127–8
- [73] Jones T B 1995 *Electromechanics of Particles* (Cambridge: Cambridge University Press)
- [74] Haus H A and Melcher J R 1989 *Electromagnetic Fields and Energy* (Englewood Cliffs, NJ: Prentice-Hall)
- [75] Knollman G C, Bellin J L S, Weaver J and Hartog J J 1971 Variable-focus liquid-filled hydroacoustic lens *J. Acoust. Soc. Am.* **49** 91
- [76] Nguyen N-T 2010 Micro-optofluidic lenses: a review *Biomicrofluidics* **4** 031501
- [77] Tsai C G, Chen C-N, Cheng L-S, Cheng C-C, Yang J-T and Yeh J A 2009 Planar liquid confinement for optical centering of dielectric liquid lenses *IEEE Photon. Technol. Lett.* **21** 1396–8
- [78] Yang C-C, Yang L, Tsai C G, Jou P H and Yeh J A 2012 Fully developed contact angle change of a droplet in liquid actuated by dielectric force *Appl. Phys. Lett.* **101** 182903
- [79] Ren H, Ren D and Wu S-T 2009 A new method for fabricating high density and large aperture ratio liquid microlens array *Opt. Express* **17** 24183–8
- [80] Javidi B, Jang J-S, Stern A and Kishk S 2004 Three dimensional image sensing, visualization and processing using integral imaging *Frontiers in Optics 2004/Laser Science XXII/Diffractive Optics and Micro-Optics/Optical Fabrication and Testing, OSA Technical Digest Series* (Rochester, NY: Optical Society of America) pFTuO2
- [81] Ren H, Xu S, Liu Y and Wu S-T 2011 Electro-optical properties of dielectric liquid microlens *Opt. Commun.* **284** 2122–5
- [82] Yang C-C, Tsai C-W G and Yeh J A 2011 Dynamic behaviour of liquid microlenses actuated using dielectric force *J. Microelectromech. Syst.* **20** 1143–9
- [83] Chikazawa Y and Gotoh T 2007 Variable iris using charged opaque particles *US Patent Application* 2070205671
- [84] Chang J-H, Jung K-D, Lee E, Choi M and Lee S 2012 Microelectrofluidic iris for variable aperture *Proc. SPIE* **8252** 825200 (MOEMS and Miniaturized Systems XI)
- [85] Jones T B 2001 Liquid dielectrophoresis on the microscale *J. Electrostat.* **51** 290–9
- [86] Karuwan C, Sukthang K, Wisitsoraat A, Phokharatkul D, Patthanasettakul V, Wechsato W and Tuantranont A 2011 Electrochemical detection on electrowetting-on-dielectric digital microfluidic chip *Talanta* **84** 1384–9
- [87] Hougham G G, Cassidy P E, Johns K and Davidson T 1999 *Fluoropolymers 2: Properties* (New York: Plenum)
- [88] Takizawa K, Kodama K and Kishi K 1998 Polarization-independent optical fiber modulator by use of polymer-dispersed liquid crystals *Appl. Opt.* **37** 3181–9

- [89] Campbell K, Groisman A, Levy U, Pang L, Mookherjea S, Psaltis D and Fainman Y 2004 A microfluidic 2×2 optical switch *Appl. Phys. Lett.* **85** 6119–21
- [90] Zuta Y, Goykhman I, Desiatov B and Levy U 2010 On-chip switching of a silicon nitride micro-ring resonator based on digital microfluidics platform *Opt. Express* **18** 24762–9
- [91] Reza S A and Riza N A 2009 A liquid lens-based broadband variable fiber optical attenuator *Opt. Commun.* **282** 1298–303
- [92] Chen Y, Xianyu H, Sun J, Kula P, Dabrowski R, Tripathi S, Twieg R J and Wu S-T 2011 Low absorption liquid crystals for mid-wave infrared applications *Opt. Express* **19** 10843–8
- [93] Wu S-T, Margerum J D, Meng H B, Hsu C S and Dalton L R 1994 Potential liquid crystal mixtures for CO₂ laser application *Appl. Phys. Lett.* **64** 1204–6
- [94] Lee J-H, Liu D N and Wu S-T 2008 *Introduction to Flat Panel Display* (New York: Wiley)
- [95] Yeh P and Gu C 1999 *Optics of Liquid Crystal Displays* (New York: Wiley)
- [96] Yang D K, West J L, Chien L C and Doane J W 1994 Control of reflectivity and bistability in displays using cholesteric liquid crystals *J. Appl. Phys.* **76** 1331–3
- [97] Fuh A Y-G, Chen C-C, Liu C-K and Cheng K-T 2009 Polarizer-free, electrically switchable and optically rewritable displays based on dye-doped polymer-dispersed liquid crystals *Opt. Express* **17** 7088–94
- [98] Lin Y-H, Yang J-M, Lin Y-R, Jeng S-C and Liao C-C 2008 A polarizer-free flexible and reflective electrooptical switch using dye-doped liquid crystal gels *Opt. Express* **16** 1777–85
- [99] Tang C W and VanSlyke S A 1987 Organic electroluminescent diodes *Appl. Phys. Lett.* **51** 913–5
- [100] Burrows P E, Gu G, Bulovic V, Shen Z, Forrest S R and Thompson M E 1997 Achieving full-color organic light-emitting devices for lightweight, flat-panel displays *IEEE Trans. Electron Devices* **44** 1188–203
- [101] Dalisa A L 1977 Electrophoretic display technology *IEEE Trans. Electron Devices* **24** 827–34
- [102] Crowley J M, Sheridan N K and Romano L 2002 Dipole moments of gyration balls *J. Electrostat.* **55** 247–59
- [103] Higuchi E and Koike Y 2001 Surface light source device and asymmetrical prism sheet *US Patent* 6222689